

PAPER

Comparison of optoelectrical characteristics between Schottky and Ohmic contacts to β -Ga₂O₃ thin film

To cite this article: Zeng Liu *et al* 2020 *J. Phys. D: Appl. Phys.* **53** 085105

View the [article online](#) for updates and enhancements.



IOP | ebooks™

Bringing you innovative digital publishing with leading voices to create your essential collection of books in STEM research.

Start exploring the [collection](#) - download the first chapter of every title for free.

Comparison of optoelectrical characteristics between Schottky and Ohmic contacts to β -Ga₂O₃ thin film

Zeng Liu¹, Yusong Zhi¹, Shan Li¹, Yuanyuan Liu^{2,5}, Xiao Tang³, Zuyong Yan¹, Peigang Li¹, Xiaohang Li³, Daoyou Guo⁴, Zhenping Wu¹ and Weihua Tang¹

¹ Laboratory of Information Functional Materials and Devices, School of Science and State Key Laboratory of Information Photonics and Optical Communications, Beijing University of Posts and Telecommunications, Beijing 100876, People's Republic of China

² Center of Materials Science and Optoelectronics Engineering, University of Chinese Academy of Sciences, Beijing 100049, People's Republic of China

³ Advanced Semiconductor Laboratory, King Abdullah University of Science and Technology (KAUST), Thuwal 23955-6900, Saudi Arabia

⁴ Center for Optoelectronics Materials and Devices, Department of Physics, Zhejiang Sci-Tech University, Hangzhou 310018, People's Republic of China

⁵ The Engineering Research Center for Semiconductor Integrated Technology, Institute of Semiconductors, Chinese Academy of Sciences, Beijing 100083, People's Republic of China

E-mail: zengliu@bupt.edu.cn, pgli@bupt.edu.cn and whtang@bupt.edu.cn

Received 24 October 2019, revised 19 November 2019

Accepted for publication 20 November 2019

Published 13 December 2019



Abstract

Schottky and Ohmic contacts are key matters affecting carrier transport in oxide semiconductor-based electrical and optical devices. For Ga₂O₃, the comparison of optoelectrical behaviors and the fundamental physical mechanism between these two contacts are not well known yet. In this work, β -Ga₂O₃ thin films were grown via metal–organic chemical vapor deposition then deposited with symmetrical Ni/Au (Schottky) or Ti/Au (Ohmic) contacts. Optoelectrical measurements show that the Ohmic contacted device exhibits superior responsivities thanks to its higher photocurrents. Meanwhile, for the Schottky contacted device, firstly, it has a faster response speed, and secondly it exhibits larger photo-to-dark current ratios owing to their low dark current. Specifically, the voltage- and light intensity-dependent responsivity and detectivities of the Schottky and Ohmic contacted devices were measured and discussed under the consideration of different voltages and UV light intensities.

Keywords: β -Ga₂O₃, Schottky and Ohmic contacts, optoelectrical characteristics, metal–organic chemical vapor deposition (MOCVD)

(Some figures may appear in colour only in the online journal)

1. Introduction

Due to the promising applications in information communications, chemical/biological analysis, flame detection, and environmental protection, ultraviolet (UV) photodetectors have drawn extensive research interest in the past few years. Among them, the UV solar-blind detectors operating in a

wavelength range from 200 nm to 280 nm are a solid choice for ozone sensing with a low false alarming rate [1–3]. The performances of photodetectors, to a large degree, depend on the nature and modified properties of the selected materials [4]. Specifically, as one of the typical wide bandgap semiconductors, β -Ga₂O₃ not only has a ultra-wide bandgap of 4.5–4.9 eV (responding in the UV solid-blind regime),

but also a high thermal and chemical stability, high critical breakdown field of 6–8 MV/cm (allowing high voltage and strong radiation operations) [5, 6], therefore allowing them to be extensively employed to fabricate UV solar-blind photodetectors [7] in the form of thin films [8–12], bulk single crystals [13–16], nanostructures [17–20] and heterogeneous structures [20–26].

A metal–semiconductor–metal (MSM) structure is a typically and widely used electrode pattern in photodetectors [27], in which either Ohmic or Schottky metal–semiconductor (M–S) contacts are employed in line with the requirements of the applications. The Ohmic contacted detectors (regarded as radiation-sensitive resistors), referenced as photoconductive, are presented by the change of resistance of the materials due to the external light stimulation, showing the intrinsic feature of materials [1, 8, 28, 29]. Meanwhile, the Schottky contacted detectors could show some modified performances owing to the efficient control of carrier transport via tuning the M–S interface barrier and the thickness of the depletion layer at the M–S interface [29–31]. For instance, Guo *et al* grew a β -Ga₂O₃ thin film by laser molecular beam epitaxy and displayed a good Ohmic electrical behavior with dark current of 45 nA and a rise time of 1.91 s, while the Schottky M–S behavior was illustrated after annealing, and the dark current and rise time were changed to be 0.3 nA and 0.62 s, respectively [8]. Other than the semiconductor and/or device processing, the contacting types depend on the choice of contacted metals [32], i.e. the difference between the work function of metal and the electron affinity of Ga₂O₃. An *et al* achieved good Ohmic contact in their photodetector; this device showed decent photoresponsivity and wavelength selectivity, while a long response time of 19 s [33]. As opposed to this, Chen *et al* demonstrated a fast responding Au/ β -Ga₂O₃ nanowires array photodetector with a faster decay time of 64 μ s [34]. Such a UV detector may have contributed to the development of a depletion layer at the Au/ β -Ga₂O₃ interface, which could restrain the separation of electron-hole pairs and conduce to the practicability more easily. In all, the M–S contact is a vital matter to determine the carrier transport and then affect the detector performances [35–39], due to the differences between the work function of metals and electron affinity of Ga₂O₃. However, to the best of our current knowledge, a systematic comparison of Schottky and Ohmic contacts to Ga₂O₃ and the influences on photodetector performances are less reported.

In this work, β -Ga₂O₃ thin films were grown via metal–organic chemical vapor deposition (MOCVD) then deposited with Ni/Au (Schottky) or Ti/Au (Ohmic) contacts. The optoelectrical behaviors, photogenerated currents, time-dependent photoresponse, photoreponsivities, detectivities and response time were systematically measured on the as-prepared devices. These aforementioned performances of the Ni/Au (Schottky) and Ti/Au (Ohmic) contacted devices were systematically compared and discussed. In addition, the inherent physical mechanism of this practical phenomenon was elucidated for further optoelectronic applications.

2. Experimental

The deposition of β -Ga₂O₃ thin film on a *c*-plane sapphire substrate was performed via a customized MOCVD thin film growth system with a close-coupled showerhead reactor. Triethylgallium (TEGa) and high-purity (5N) oxygen gas were used as gallium and oxygen sources, respectively. TEGa was stored in a stainless steel bubbler, which was kept at temperature of 35 °C and pressure of 760 Torr. Oxygen gas was delivered into the growth chamber, and a gas ratio of 6000 SCCM was set. On the basis of the set oxygen flow, the [O/Ga] molar ratio was regulated to be ~ 1657 . Specifically, according to the Antoine's equation $\log(P_{\text{MO}}) = a - b/T$ [40, 41], where P_{MO} is the vapor pressure of TMGa, a and b are the Antoine constants, and T is the thermodynamic temperature of TMGa. $n_{\text{mo}} = \frac{F \times P_{\text{MO}}}{V_{\text{m}} \times (P_{\text{bub}} - P_{\text{MO}})}$, where n_{mo} is the molar flow rate of TMGa, F is the flow rate of carrier gas, $V_{\text{m}} = 22414 \text{ cm}^3 \text{ mol}^{-1}$ (ideal gas molar volume), P_{bub} is the pressure inside the bubbler. $n_{\text{O}_2} = \frac{F_{\text{O}_2}}{V_{\text{m}}}$, where n_{O_2} is the molar flow rate of O₂, and F_{O_2} is the flow rate of O₂. Therefore, the [O/Ga] molar ratios in the experiment could be expressed as: $[\text{O/Ga}] = \frac{n_{\text{O}_2}}{n_{\text{mo}}} = \frac{5.35 \times 10^{-1}}{3.23 \times 10^{-4}} \sim 1657$. The growth process was maintained for 15 min under a fixed growth chamber condition with a temperature of 735 °C and pressure of 25 Torr.

The symmetrical Ni/Au and/or Ti/Au metal electrodes were patterned on the surface of β -Ga₂O₃ thin film by means of electron beam evaporation, conventional photolithography and lift-off techniques. The same photomask was employed to pattern the Ni/Au (120 nm/180 nm) and Ti/Au (120 nm/180 nm) metal electrodes. The quadrate electrodes are 400 μ m wide and 400 μ m long, and 200 μ m spacing gap. Calculated from the scale of electrode patterns, the efficient irradiant area could be about $8 \times 10 \mu\text{m}^2$ for both electrode types. In detail, after patterning the Ti/Au electrodes, the fabricated devices were annealed in N₂ at 200 °C for 60 s, in order to achieve better Ohmic contacts [42]. Before the Ni/Au electrodes deposition, the β -Ga₂O₃ thin film was surface treated by O₂ plasmas for 30 s [43–45]. This is because the Schottky contacts on oxide semiconductors are often challenged by the distinct surface charge accumulation layer [42, 44–48]. The metal–semiconductor contact region is a key issue for the successful fabrication of Schottky contacts on various oxide semiconductors, including β -Ga₂O₃ studied in this work. The O₂ plasmas treatments allow us to increase the oxygen content at the Ni/ β -Ga₂O₃ interface, inducing interface charge reduction for Ni contacts on the surface of β -Ga₂O₃ and the improvement of Schottky characteristics [43, 46, 49, 50]. The current–voltage (*I*–*V*) characteristics are performed with a Keithley 4200 semiconductor parameter analyzer. The measurement of time-dependent photoresponse is finished by using an UV lamp with various intensities through tuning the distance between measuring sample and the UV light source, and the UV light intensities could be read by a light receptor and a display instrument. The crystal structure of the β -Ga₂O₃ thin film was analyzed by a Bruker D8 Advance x-ray diffractometer

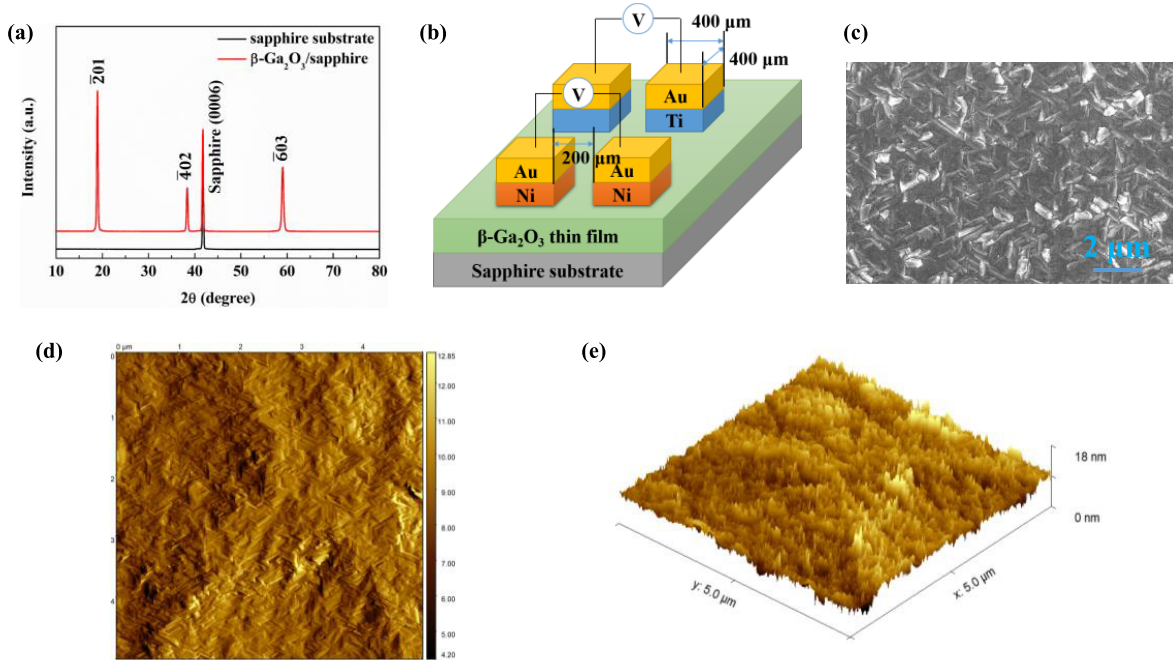


Figure 1. (a) The XRD pattern of the MOCVD-grown β -Ga₂O₃ thin film, (b) the schematic diagram of the fabricated β -Ga₂O₃ thin film based MSM structured UV solar-blind photodetector. (c) The SEM image of the surface of the β -Ga₂O₃ thin film. (d) Plane AFM surface morphology image of the β -Ga₂O₃ thin films with $5 \times 5 \mu\text{m}^2$ scanning area, and the tridimensional AFM image is displayed in (e).

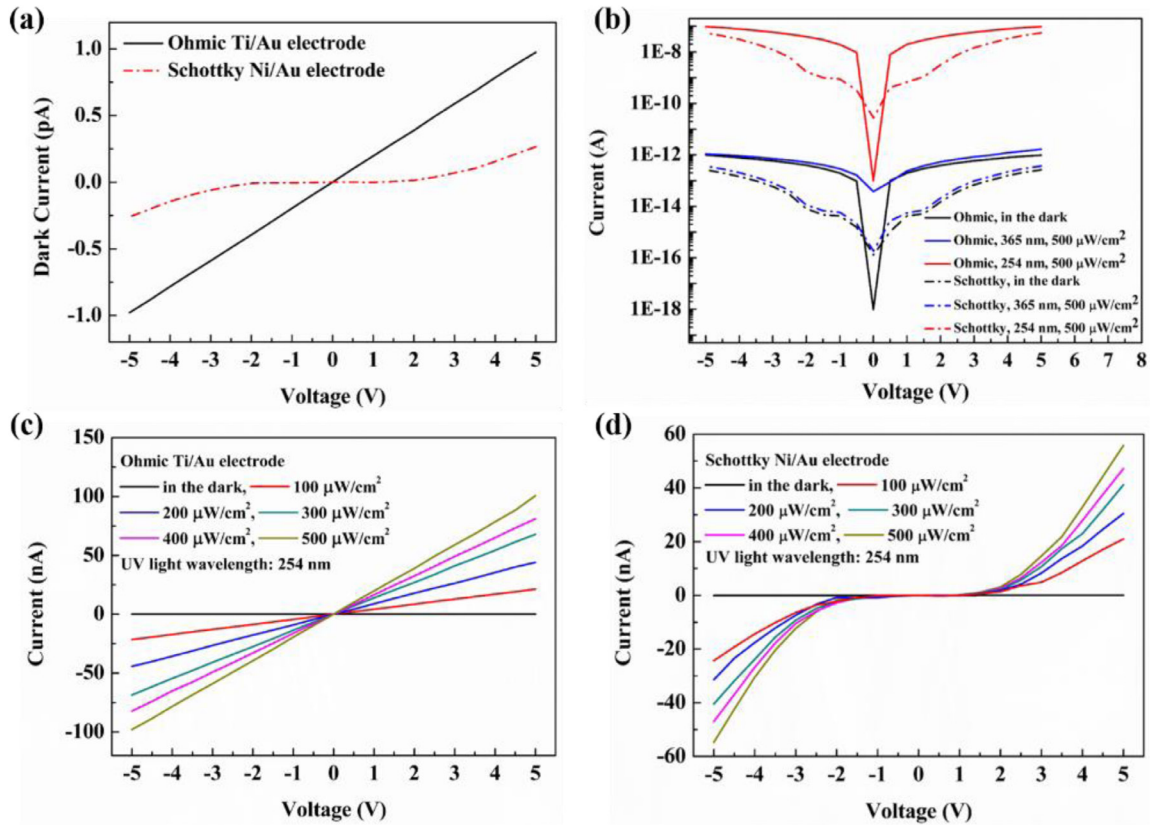


Figure 2. (a) The linear-scale I - V characteristics of the MOCVD-grown β -Ga₂O₃ thin film-based photodetector in the dark for Schottky Ni/Au (red dot line) and Ohmic Ti/Au contacts (black full line). (b) The semi log-scale I - V characteristics of both the Schottky (Ni/ β -Ga₂O₃/Ni) and Ohmic (Ti/ β -Ga₂O₃/Ti) devices in the dark, under the 254 nm and 365 nm UV light illuminations with intensities of 500 $\mu\text{W cm}^{-2}$. The linear-scale I - V curves of (c) Ohmic devices and (d) Schottky devices in the dark and under the 254 nm UV light illuminations with intensities from 100 $\mu\text{W cm}^{-2}$ to 500 $\mu\text{W cm}^{-2}$, step is 100 $\mu\text{W cm}^{-2}$.

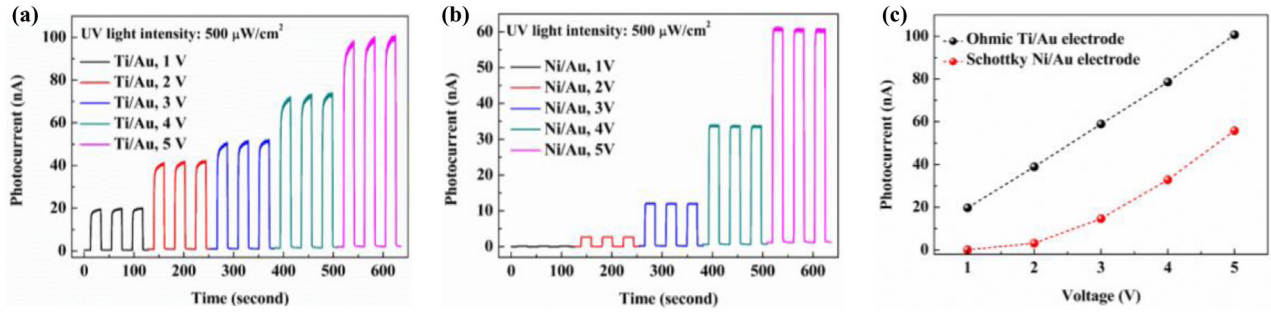


Figure 3. The continuous time-dependent photoresponse of the β -Ga₂O₃ thin film grown by MOCVD at voltages from 1 V to 5 V under the 254 nm UV light illumination with a light intensity of 500 μ W cm⁻² for (a) Ohmic devices and (b) Schottky devices. (c) The voltage-dependent photocurrents under the 254 nm UV light illumination with a light intensity of 500 μ W cm⁻².

(XRD) with Cu K α ($\lambda \sim 1.5405$ Å) radiation. All the measurements in this work were executed in air at room temperature.

3. Results and discussion

As shown in figure 1(a), the XRD pattern of the β -Ga₂O₃ thin film grown by MOCVD on *c*-plane sapphire substrate indicates a good single crystallinity with highly ordered peaks along the (201), (402) and (603) directions (JCPDS #43-1012), except for the sharp (0006) peak from the sapphire substrate (JCPDS #46-1212). Figure 1(b) shows a schematic diagram of the fabricated β -Ga₂O₃ thin film-based MSM structured UV solar-blind photodetector. The side length of the quadrate electrode pattern is 400 μ m, and the spacing distance between two symmetrical electrodes is 200 μ m. So, the efficient UV light radiant area (*S*) could be calculated to be 8×10^4 μ m². As key influences on devices output performances, the morphological information of the used β -Ga₂O₃ thin film is provided. The scanning electron microscope (SEM) image is displayed in figure 1(c), where the uniformly claviform grains with well-defined boundaries provide good crystallization of the prepared β -Ga₂O₃ thin film. The plane and tridimensional atomic force microscope (AFM) images are shown in figures 1(d) and (e), respectively, and the root mean square (RMS) roughness is 1.234 nm.

Figure 2(a) shows the dark *I*-*V* characteristics of the typical back-to-back MSM structured Schottky and Ohmic β -Ga₂O₃ thin film-based UV solar-blind photodetectors, in the voltage range from -5 V to 5 V. The good symmetrical *I*-*V* curves suggest a good quality and uniform β -Ga₂O₃ thin film, and consistent electrode patterns. At an applied voltage of 5 V, the dark current (*I*_{dark}) of the Schottky and Ohmic devices are 2.65×10^{-13} A and 9.77×10^{-13} A, respectively. The *I*_{dark} obtained from Schottky devices is more than four times lower than that from Ohmic devices, due to the efficient constraint of carriers (electrons) transport by the interface barrier of Ni/ β -Ga₂O₃, instead of the light sensitive *I*-*V* behaviors like a resistor [1, 29]. As seen from figure 2(b), the photocurrent (*I*_{photo}) at 5 V is 5.58×10^{-8} A and 9.76×10^{-8} A for Schottky and Ohmic devices, respectively, and accordingly the photo-to-dark current ratio [$(I_{\text{photo}} - I_{\text{dark}})/I_{\text{dark}}$] at 5 V is $\sim 2.1 \times 10^5$ and $\sim 1.0 \times 10^5$. The photoresponse, $(I_{\text{photo}} - I_{\text{dark}})/I_{\text{dark}}$, in the Schottky device is superior to that in Ohmic devices, which

is consistent with the description in [8]. Meanwhile, the *I*-*V* curves of both the Ohmic and Schottky contacted photodetectors are shown in figures 2(c) and (d), respectively. Larger UV light intensities contribute to larger *I*_{photo} for both two-typed devices. The ‘shoulders’ in the semi-log scale *I*-*V* curves of Schottky devices in figure 2(b) may be due to the non-uniformity Schottky barriers [51]. As indicated in figure 2(c), the *I*_{photo} of the Ohmic device exhibits a good linear characteristic, suggesting a great stability of UV light response. The incident photons are absorbed in the β -Ga₂O₃ thin film and change the electronic energy distribution, leading to a disciplinary and linear increase of *I*_{photo} [1]. The high $(I_{\text{photo}} - I_{\text{dark}})/I_{\text{dark}}$ of $\sim 10^5$ and the excellent linearity of *I*_{photo} verify that the photodetectors presented in this work are sensitive and stable. In addition to the results in figure 2(b), the photocurrent under the 365 nm UV light illumination shows a small increase. Compared to that in the dark, the small increase may be due to the defects in β -Ga₂O₃ thin film and/or the unpurified UV light source [14]. This little variation between 365 nm light illumination and dark condition suggests an outstanding wavelength selectivity, in comparison to the sharp increasing *I*_{photo} under 254 nm UV light illumination.

Figure 3 shows the time-dependent photoresponse and the voltage-dependent *I*_{photo} of the β -Ga₂O₃ thin film grown by MOCVD at voltages from 1 V to 5 V under the 254 nm UV light illumination with a light intensity of 500 μ W cm⁻². The *I*_{photo} increase with the applied voltage increase for both Schottky and Ohmic contacted photodetectors, which can be clearly seen in figures 3(a) and (b). As indicated by figure 3(c), the *I*_{photo} in Ohmic devices are higher than that in Schottky devices. Taking the time-dependent *I*_{photo} (5 V and 500 μ W cm⁻²) as an example, the rise and decay time (τ_r and τ_d) of the devices are exhibited and discussed, as displayed in figure 4. In figures 4(a) and (b), the fitting of the time-dependent photoresponding curves are according to an exponential relaxation equation [52]:

$$I = I_0 + Ae^{-t/\tau} \quad (1)$$

where *I*₀ is the stable state photocurrent, *A* is a constant, *t* is the time, and τ is a relaxation time constant. τ_r and τ_d are the rise and decay edge of the time constants, respectively. In addition, the *I*_{photo} at different voltages ranging from 1 V to 5 V are shown in figure 3(c). The τ_r and τ_d of Ohmic devices are larger than that of Schottky devices, suggesting a faster

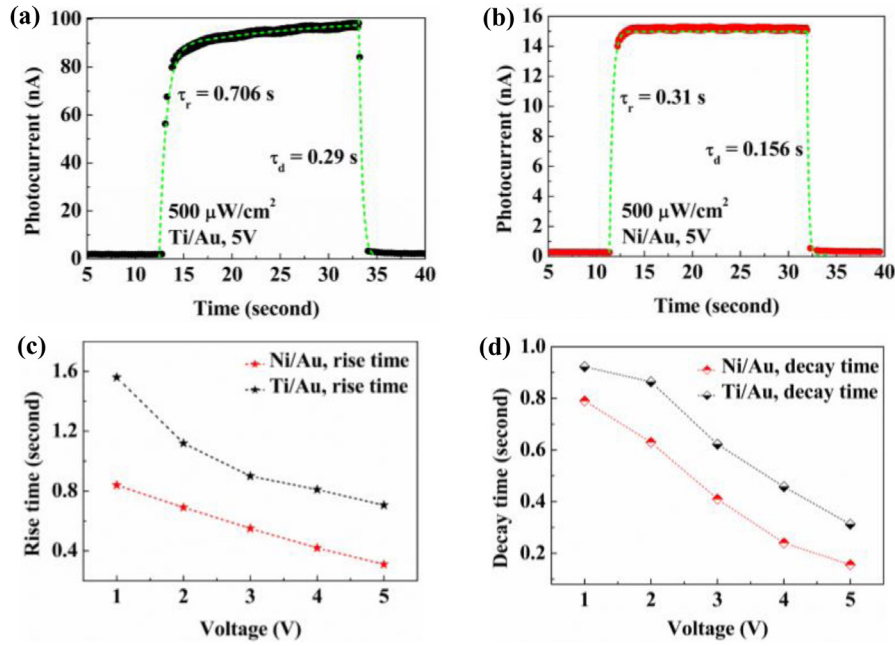


Figure 4. The rise and decay time of the $\beta\text{-Ga}_2\text{O}_3$ thin film based photodetector of (a) Ohmic devices and (b) Schottky devices responding to the 254 nm UV light with a light intensity of $500 \mu\text{W cm}^{-2}$ at 5 V, with Ti/Au and Ni/Au electrodes, respectively. The voltage-dependent (c) rise time and (d) decay time for Schottky and Ohmic devices.

photoresponse of Schottky devices compared to that of the Ohmic devices. The faster photoresponse in Schottky devices verifies a rapid change of electron concentration as soon as the UV light is radiated on the surface of the $\beta\text{-Ga}_2\text{O}_3$ thin film, while the slower photoresponse of Ohmic devices may be due to the electron traps at the M–S interface, caused by some defects at the M–S interface and/or in the $\beta\text{-Ga}_2\text{O}_3$ thin film. What could be clearly seen in figures 4(a) and (b) is that the rise edge and decay edge for Schottky and Ohmic devices are obviously different. Using equation (1), the τ_r and τ_d of Ohmic devices are 0.706 s and 0.29 s, respectively, which are larger than those of 0.31 s and 0.156 s of Schottky devices. In detail, the voltage-dependent response time is given in figures 4(c) and (d), while the τ_r and τ_d presented here indicate that the Schottky device has a faster photoresponse than the Ohmic devices at the applied voltage range from 1 V to 5 V. Moreover, for these two typed devices, the larger applied voltages could achieve a faster photoresponse, i.e. smaller τ_r and τ_d , owing to the larger kinetic energy that electron acquired from higher voltages [12]. In general, the fast light response could be attributed to the rapid change of the electron concentration of the $\beta\text{-Ga}_2\text{O}_3$ thin film as soon as the UV light was turned on and/or off. For Ohmic (Ti/Au) devices, the response process was deeply affected by the interface trapping and oxygen vacancies defects, therefore, the rise and decay time of the Ohmic devices are long. However, for the Schottky (Ni/Au) devices after O_2 plasmas treatment at the Ni/ $\beta\text{-Ga}_2\text{O}_3$ interface, decent Schottky electrical behaviors were obtained, and the electrons can also be photogenerated and recombined faster than that of the Ohmic devices, due to the weaker influences of traps and defects on the light responses [8, 53–55].

As reported, the band structure of $\beta\text{-Ga}_2\text{O}_3$ along a continuous path in the Brillouin zone has been studied [56–59].

According to these results, the conduction-band minimum $\beta\text{-Ga}_2\text{O}_3$ material is located at the Γ point, and the corresponding bandgap is only about 0.04 eV larger than those at other points in the band structure [57]. In addition, the secondary conduction bands at Z and Y points just have minimal values, as well as the minima at N and X points. So, the bandgap of $\beta\text{-Ga}_2\text{O}_3$ is direct with an acceptable deviation [56–59] at every point in its energy band structure. For understanding the inherent physical mechanism of the operating Schottky Ni/Au contacted and Ohmic Ti/Au contacted $\beta\text{-Ga}_2\text{O}_3$ photodetectors, the systematic band diagrams of $\beta\text{-Ga}_2\text{O}_3$ with Ti and Ni in the dark and under the 254 nm UV light illumination are shown in figures 5(a)–(d). The work functions of Ti and Ni [$\Phi(\text{Ti})$ and $\Phi(\text{Ni})$] are 4.33 eV and 5.15 eV, respectively, and the electron affinity of $\beta\text{-Ga}_2\text{O}_3$ [$\chi(\beta\text{-Ga}_2\text{O}_3)$] is about 4.00 eV as reported [60–62]. So, the interface barriers of $\beta\text{-Ga}_2\text{O}_3$ with Ti and Ni ($\Delta\varphi_{\text{Ti}-\beta\text{-Ga}_2\text{O}_3}$ and $\Delta\varphi_{\text{Ni}-\beta\text{-Ga}_2\text{O}_3}$) could be calculated to be 0.33 eV and 1.15 eV, on the basis of the Schottky–Mott rule [29, 30]. The puny interface barrier between Ti and $\beta\text{-Ga}_2\text{O}_3$ contributes to the Ohmic M–S contact, while the larger interface barrier between Ni and $\beta\text{-Ga}_2\text{O}_3$ leads to the Schottky M–S contact. The I – V behavior of Ohmic devices could be expressed by the electron tunneling, while for the Schottky contact, the I – V characteristic could be described by the thermionic emission (TE) theory [63–65]:

$$J = J_0(\exp\left(\frac{qV}{nkT}\right) - 1) \quad (2)$$

and

$$J_0 = A^*T^2 \exp(-\varphi_B/kT), \quad (3)$$

where J_0 is the saturation current density, A is the area of M–S contact, A^* is the efficient Richardson

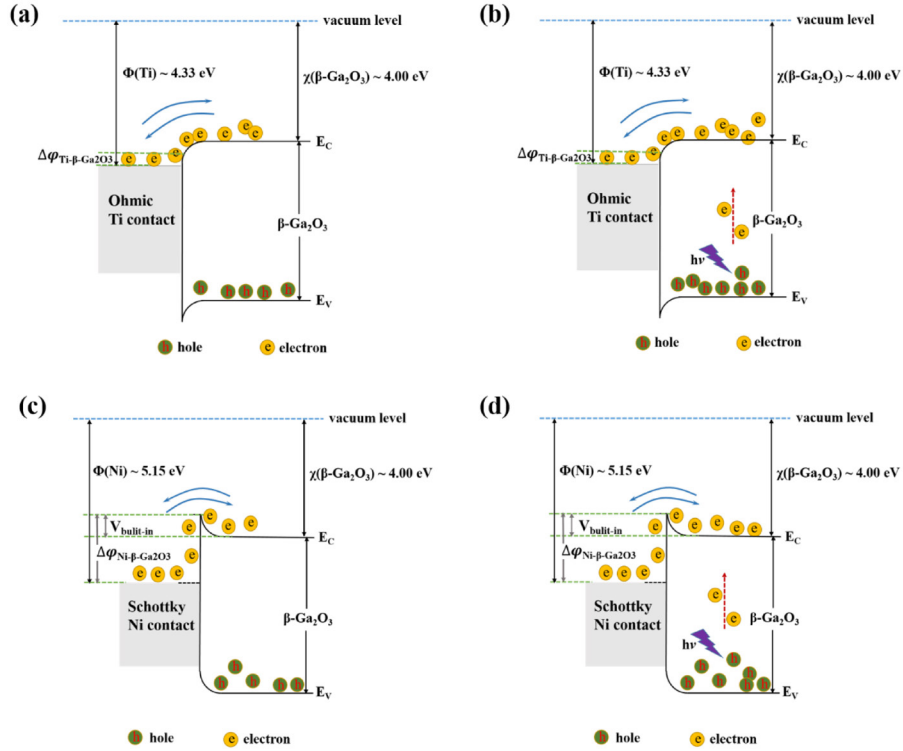


Figure 5. Band diagram of the β -Ga₂O₃ with Ti (a) in the dark and (b) under the 254 nm light illumination. Band diagram of the β -Ga₂O₃ with Ni (c) in the dark and (d) under the 254 nm light illumination.

constant ($A^* = \frac{4\pi q m^* k^2}{h^3} = 41.1 \text{ A}(\text{cm}^2 \cdot \text{K}^2)^{-1}$) by taking m^* of $0.342m_0$, m_0 is the free electron mass of β -Ga₂O₃ [66, 67], k is Boltzmann constant, and φ_B is the barrier height, expressed as $\varphi_B = \frac{kT}{q} \ln(\frac{A^* T^2}{J_0})$. As displayed in figure 5, the built-in electrical field ($V_{\text{built-in}}$) is developed when the Ni and β -Ga₂O₃ contact each other. In the dark, as shown in figures 5(a) and (c), the larger interface barrier in Schottky device could restrict electron transport across the Ni/ β -Ga₂O₃ interface, while the Ohmic device is almost like a radiation (UV light)-sensitive resistor with a tiny interface barrier. Therefore, the I_{dark} in Ohmic device is larger than that in the Schottky device as displayed in figure 2(a), and the Schottky device may be more sensitive to the small signal owing to its smaller I_{dark} . Under 254 nm UV light illuminations, as displayed in figure 5(b) and (d), the incident photons with energy ($h\nu$) greater than the energy bandgap of the β -Ga₂O₃ thin film could be absorbed by the β -Ga₂O₃ material and then produce the photo-generated electron-hole pairs (electrons at valence band are motivated to the conduction band by absorbed photons, and correspondingly holes are produced at the valence band), thereby changing the electrical conductivity of β -Ga₂O₃. Given a voltage, the electrons in β -Ga₂O₃ are pushed to the conduction band, while the holes are driven to the valence band. For Ohmic Ti/Au contacted β -Ga₂O₃ photodetector studied here, the I_{photo} is linearly improved by the incident 254 nm UV light, while for the Schottky Ni/Au contacted β -Ga₂O₃ photodetector, the I - V characteristics show Schottky (rectifying) behavior owing to the interface barrier between Ni metal electrode and β -Ga₂O₃ thin film. This phenomenon

could be obtained whether the 254 nm UV light is turned on or not [1].

For photodetectors, responsivity (R) and detectivity (D^*) are two vital parameters to evaluate the detector performances and can be described as the following relationships [68]:

$$R = \frac{I_{\text{photo}} - I_{\text{dark}}}{P_{\text{light}} \cdot S} \quad (4)$$

and

$$D^* = \frac{R_{254}}{\sqrt{2qI_{\text{dark}}/S}}, \quad (5)$$

where P_{light} is the UV light intensity used in the measurements, S is the efficient radiant area in devices, and R_{254} is the photo responsivity under 254 nm light illumination. According to equations (4) and (5), the R and D^* by different driven voltages and light intensities are displayed in figures 6(a)–(d) for Schottky and Ohmic β -Ga₂O₃ thin film-based UV solar-blind photodetectors. As can be seen from figure 6(a), with the UV light intensity of $500 \mu\text{W cm}^{-2}$, the responsivities increase with the increasing voltages from 1 V to 5 V, for both the Schottky (from 1.68 mA W^{-1} to 0.14 A W^{-1}) and Ohmic (from 49 mA W^{-1} to 0.25 A W^{-1}) devices. The responsivities for Ohmic devices ranging from 1 V to 5 V are all higher than those of Schottky devices, due to the larger I_{photo} of Ohmic devices compared to the Schottky devices, as well as the same P_{light} intensities and S , following the description in equation (4). In addition to the responsivities with different UV light intensities, the R of Ohmic devices are also higher than those of Schottky devices, as shown in figure 6(c). The

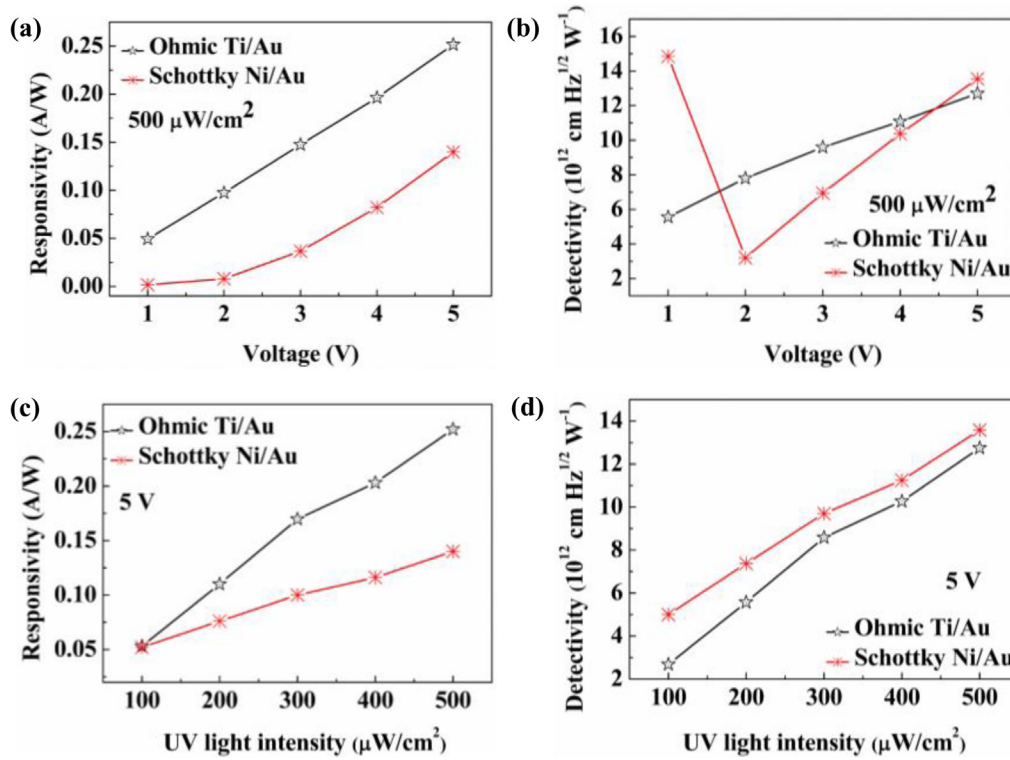


Figure 6. The voltage-dependent (a) responsivity and (b) detectivity for both Schottky Ni/Au and Ohmic Ti/Au contacted $\beta\text{-Ga}_2\text{O}_3$ thin film-based UV solar-blind photodetectors with 254 nm UV light intensity of 500 $\mu\text{W cm}^{-2}$ from 1 V to 5 V with a step of 1 V. The UV light intensity-dependent (c) responsivity and (d) detectivity for both Schottky Ni/Au and Ohmic Ti/Au contacted $\beta\text{-Ga}_2\text{O}_3$ thin film based UV solar-blind photodetectors at 5 V with 254 nm UV light intensities from 100 $\mu\text{W cm}^{-2}$ to 500 $\mu\text{W cm}^{-2}$ with a step of 100 $\mu\text{W cm}^{-2}$.

responsivities are increased by the increasing light intensity. By contrast, the Ohmic device could make more photogenerated electron-hole pairs to generate I_{photo} than the Schottky devices [1, 69–72].

The detectivities are governed by responsivities and the square root of I_{dark} for a photodetector, as given in equation (5). As shown in figure 6(b), the D^* of Schottky devices are larger than that of Ohmic devices, owing to superlow I_{dark} (3.2×10^{-16} A) of Schottky devices at 1 V, which should contribute to the rectifying effect caused by the Ni/ $\beta\text{-Ga}_2\text{O}_3$ interface barrier. In comparison, the D^* of the Schottky device at 2 V to 5 V are obviously smaller than that at 1 V; this trend is in accordance with the rectifying I - V curves in figure 2(d). For Ohmic devices, the I_{dark} is always kept at $\sim 10^{-13}$, so the D^* have the same evolutive tendency with R as displayed in figure 6(a). In figure 6(d), the D^* of Schottky devices are slightly larger than those of Ohmic devices at 5 V with 254 nm UV light intensity from 100 $\mu\text{W cm}^{-2}$ to 500 $\mu\text{W cm}^{-2}$ with a step of 100 $\mu\text{W cm}^{-2}$, in accordance with the results in figure 6(b) at 5 V, indicating a better characterizing parameter for normalizing signal-to-noise ratio [1].

4. Conclusions





In summary, in this study, we grew a $\beta\text{-Ga}_2\text{O}_3$ thin film by using the metal-organic chemical vapor deposition technique, and made a comparison of optoelectrical properties of the prepared $\beta\text{-Ga}_2\text{O}_3$ thin films with Schottky Ni/Au and Ohmic Ti/Au

Au contacted electrodes. The results show that Schottky device has higher photo-to-dark current ratios and a faster photo response speed than those of the Ohmic device. Working as a UV solar-blind photodetector, the responsivities of Schottky devices are smaller than those of Ohmic devices. Owing the lower I_{dark} , the D^* of Schottky devices are superior to those of Ohmic devices at 5 V with light intensity from 100 to 500 $\mu\text{W cm}^{-2}$. What is more, with 500 $\mu\text{W cm}^{-2}$ light intensity, the different D^* from 1 V to 5 V are also discussed on the basis of the Schottky I - V behaviors. In a word, we discussed and analyzed the differences between Schottky and Ohmic contacted $\beta\text{-Ga}_2\text{O}_3$ thin film-based UV solar-blind photodetectors, and gave out some inherent physical mechanisms, in order to present the effect of metal- $\beta\text{-Ga}_2\text{O}_3$ contacted types (Schottky or Ohmic) on the devices performances, as well as their differences, operating as a UV solar-blind photodetector.

Acknowledgments

This work was supported by the National Natural Science Foundation of China (Grant Nos. 61774019, 51572033, and 51572241), the Beijing Municipal Commission of Science and Technology, China (Grant No. SX2018-04). In addition, the authors acknowledge the Fundamental Research Funds for the Central Universities and the Foundation of State Key Laboratory of Information Photonics and Optical Communications (Beijing University of Posts and Telecommunications).

ORCID iDs

Zeng Liu  <https://orcid.org/0000-0003-3215-7929>
 Xiaohang Li  <https://orcid.org/0000-0002-4434-365X>
 Daoyou Guo  <https://orcid.org/0000-0002-9126-4460>
 Zhenping Wu  <https://orcid.org/0000-0003-2986-8068>

References

- [1] Razeghi M and Rogalski A 1996 *J. Appl. Phys.* **79** 7433
- [2] Chen H, Liu K, Hu L, Al-Ghamdi A A and Fang X 2015 *Mater. Today* **18** 493
- [3] Sang L, Liao M and Sumiya M 2013 *Sensors* **13** 10482
- [4] Konstantatos G and Sargent E H 2010 *Nat. Nanotechnol.* **5** 391
- [5] Pearton S J, Yang J, Cary P H, Ren F, Kim J, Tadjer M J and Mastro M A 2018 *Appl. Phys. Rev.* **5** 011301
- [6] Liu Z, Li P G, Zhi Y S, Wang X L, Chu X L and Tang W H 2019 *Chin. Phys. B* **28** 017105
- [7] Xu J, Zheng W and Huang F 2019 *J. Mater. Chem. C* **7** 8753
- [8] Guo D Y, Wu Z P, An Y H, Guo X C, Chu X L, Sun C L, Li L H, Li P G and Tang W H 2014 *Appl. Phys. Lett.* **105** 023507
- [9] Kumar N, Arora K and Kumar M 2019 *J. Phys. D: Appl. Phys.* **52** 335103
- [10] Qin Y et al 2019 *IEEE Electron Device Lett.* **40** 1475
- [11] Xu Y et al 2019 *IEEE Trans. Electron Devices* **66** 2276
- [12] Liu Z et al 2019 *J. Mater. Chem. C* **7** 13920
- [13] Chen X et al 2019 *ACS Appl. Mater. Interfaces* **11** 7131
- [14] Dong L, Yu J, Jia R, Hu J, Zhang Y and Sun J 2019 *Opt. Mater. Express* **9** 1191
- [15] Oshima T, Okuno T, Arai N, Suzuki N, Ohira S and Fujita S 2008 *Appl. Phys. Express* **1** 011202
- [16] Chen M, Ma J, Li P, Xu H and Liu Y 2019 *Opt. Express* **27** 8717
- [17] Zou R, Zhang Z, Liu Q, Hu J, Sang L, Liao M and Zhang W 2014 *Small* **10** 1848
- [18] Wang S et al 2019 *RSC Adv.* **9** 6064
- [19] Feng W, Wang X, Zhang J, Wang L, Zheng W, Hu P, Cao W and Yang B 2014 *J. Mater. Chem. C* **2** 3254
- [20] Li Y, Tokizono T, Liao M, Zhong M, Koide Y, Yamada I and Delaunay J 2010 *Adv. Funct. Mater.* **20** 3972
- [21] An Y H, Guo D Y, Li S Y, Wu Z P, Huang Y Q, Li P G, Li L H and Tang W H 2016 *J. Phys. D: Appl. Phys.* **49** 285111
- [22] Liu Z, Wang X, Zhi Y S, Wang X L, Chu X L, Li S, Yan Z, Li P G and Tang W H 2019 *Phys. Status Solidi a* **216** 1900570
- [23] Guo D Y et al 2017 *Semicond. Sci. Technol.* **32** 03LT01
- [24] Guo D et al 2018 *ACS Nano* **12** 12827
- [25] Kong W Y, Wu G A, Wang K Y, Zhang T F, Zou Y F, Wang D D and Luo L B 2016 *Adv. Mater.* **28** 10725
- [26] Li S et al 2019 *ACS Appl. Mater. Interfaces* **11** 35105
- [27] Sze S M, Coleman D J and Loya A 1971 *Solid-State Electron.* **14** 1209
- [28] Xue H W, He Q M, Jian G Z, Long S B, Pang T and Liu M 2018 *Nanoscale Res. Lett.* **13** 290
- [29] Mott N F 1939 *Proc. R. Soc. A* **171** 27
- [30] Schottky W 1939 *Z. Phys.* **113** 367
- [31] Sze S M and Ng K K 2007 *Physics of Semiconductor Devices* (New York: Wiley)
- [32] Bae J, Kim H Y and Kim J 2017 *ECS J. Solid State Sci. Technol.* **6** Q3045
- [33] An Y H, Guo D Y, Li Z M, Wu Z P, Zhi Y S, Cui W, Zhao X L, Li P G and Tang W H 2016 *RSC Adv.* **6** 66924
- [34] Chen X, Liu K, Zhang Z, Wang C, Li B, Zhao H, Zhao D and Shen D 2016 *ACS Appl. Mater. Interfaces* **8** 4185
- [35] Cowley A M and Sze S M 1965 *J. Appl. Phys.* **36** 3212
- [36] Minc W 1970 *Surf. Sci.* **21** 443
- [37] Tung R T 1992 *Phys. Rev. B* **45** 13509
- [38] Jiao Y, Hellman A, Fang Y, Guo S and Kall M 2015 *Sci. Rep.* **5** 11374
- [39] Li J G 1997 *Mater. Chem. Phys.* **47** 126
- [40] Thomson G W 1946 *Chem. Rev.* **38** 1
- [41] Li Z, Jiao T, Hu D, Lv Y, Li W, Dong X, Zhang Y, Feng Z and Zhang B 2019 *Coatings* **9** 281
- [42] Mao S and Luo J 2019 *J. Phys. D: Appl. Phys.* **52** 503001
- [43] Michel J, Splith D, Rombach J, Papadogianni A, Berthold T, Krischok S, Grundmann M, Bierwagen O, von Wenckstern H and Himmerlich M 2019 *ACS Appl. Mater. Interfaces* **11** 27073
- [44] Yang J, Sparks Z, Ren F, Pearton S J and Tadjer M 2018 *J. Vac. Sci. Technol. B* **36** 061201
- [45] Schultz T, Vogt S, Schlupp P, von Wenckstern H, Koch N and Grundmann M 2018 *Phys. Rev. Appl.* **9** 064001
- [46] King P D C, Veal T D, Payne D J, Bourlange A, Egdel R G and McConville C F 2008 *Phys. Rev. Lett.* **101** 116808
- [47] Hmlinen J, Munnik F, Ritala M and Leskel M 2008 *Chem. Mater.* **20** 6840
- [48] Fleisch T H and Mains G J 1986 *J. Phys. Chem. A* **90** 5317
- [49] Splith D, Miller S, von Wenckstern H and Grundmann M 2018 *Proc. SPIE* **10533** 10533C
- [50] Hou C, Gazoni R M, Reeves R J and Allen M W 2019 *IEEE Electron Device Lett.* **40** 337
- [51] Jian G et al 2018 *AIP Adv.* **8** 015316
- [52] Liu N, Fang G, Zeng W, Zhou H, Cheng F, Zheng Q, Yuan L, Zou X and Zhao X 2010 *ACS Appl. Mater. Interfaces* **2** 1973
- [53] Mosbacher H L, Strzemechny Y M, White B D, Smith P E, Look D C, Reynolds D C, Litton C W and Brillson L J 2005 *Appl. Phys. Lett.* **87** 012102
- [54] Allen M W and Durbin S M 2008 *Appl. Phys. Lett.* **92** 122110
- [55] Moloney J et al 2019 *J. Phys. D: Appl. Phys.* **52** 475101
- [56] Wang X L, Quhe R G, Zhi Y S, Liu Z, Huang Y Q, Dai X Q, Tang Y N, Wu Z P and Tang W H 2019 *Superlattices Microstruct.* **125** 330
- [57] Peelaers H and Van de Walle C G 2015 *Phys. Status Solidi b* **252** 828
- [58] Varley J B, Weber J R, Janotti A and Van de Walle C G 2010 *Appl. Phys. Lett.* **97** 142106
- [59] He H, Blanco M A and Pandey R 2006 *Appl. Phys. Lett.* **88** 261904
- [60] Michaelson H B 1977 *J. Appl. Phys.* **48** 4729
- [61] Mohamed M, Irmscher K, Janowitz C, Galazka Z, Manzke R and Fornari R 2012 *Appl. Phys. Lett.* **101** 132106
- [62] Darowicki K, Krakowiak S and Slepiski P 2006 *Electrochim. Acta* **51** 2204
- [63] Furno M, Bonani F and Ghione G 2007 *Solid-State Electron.* **51** 466
- [64] Latreche A 2019 *SN Appl. Sci.* **1** 188
- [65] Harada T, Ito S and Tsukazaki A 2019 *Sci. Adv.* **5** eaax5733
- [66] He H, Orlando R, Blanco M A, Pandey R, Amzallag E, Baraille I and Rerat M 2006 *Phys. Rev. B* **74** 195123
- [67] Sasaki K, Higashiwaki M, Kuramata A, Masui T and Yamakoshi S 2013 *IEEE Electron Device Lett.* **34** 493
- [68] Gong X, Tong M, Xia Y, Cai W, Moon J S, Cao Y, Yu G, Shieh C L, Nilsson B and Heeger A J 2009 *Science* **325** 1665
- [69] Rose A 1963 *Concepts in Photoconductivity and Allied Problems* (New York: Interscience)
- [70] Rettie A J E, Chemelewski W D, Emin D and Mullins C B 2016 *J. Phys. Chem. Lett.* **7** 471
- [71] Kokum A F, Miranowicz A, Liberato S D, Savasta S and Nori F 2019 *Nat. Rev. Phys.* **1** 19
- [72] Latreche A and Ouennoughi Z 2013 *Semicond. Sci. Technol.* **28** 105003